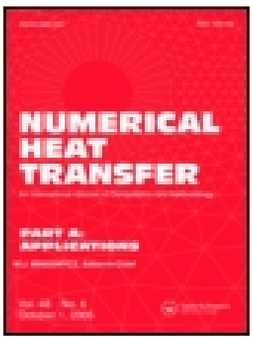

Numerical Heat Transfer, Part A: Applications

ISSN: 1040-7782 (Print) 1521-0634 (Online) Journal homepage: http://www.tandfonline.com/loi/unht20

CONJUGATE COMPUTATION OF TRANSIENT FLOW AND HEAT AND MASS TRANSFER BETWEEN HUMID AIR AND DESICCANT PLATES AND CHANNELS

Hassan S. Al-Sharqawi & Noam Lior

To cite this article: Hassan S. Al-Sharqawi & Noam Lior (2004) CONJUGATE COMPUTATION OF TRANSIENT FLOW AND HEAT AND MASS TRANSFER BETWEEN HUMID AIR AND DESICCANT PLATES AND CHANNELS, Numerical Heat Transfer, Part A: Applications, 46:6, 525-548, DOI: 10.1080/10407780490487957

To link to this article: http://dx.doi.org/10.1080/10407780490487957

Published online: 17 Aug 2010.

Numerical Heat Transfer, Part A, 46: 525–548, 2004

ISSN: 1040-7782 print/1521-0634 online
DOI: 10.1080/10407780490487957

Taylor & Francis
Taylor & Francis Group

CONJUGATE COMPUTATION OF TRANSIENT FLOW AND HEAT AND MASS TRANSFER BETWEEN HUMID AIR AND DESICCANT PLATES AND CHANNELS

Hassan S. Al-Sharqawi and Noam Lior
Department of Mechanical Engineering and Applied Mechanics, University of Pennsylvania, Philadelphia, Pennsylvania, USA

This is a numerical study of dehumidification of humid air in laminar and turbulent flows ($333 \le \mathrm{Re} \le 6{,}000$) over desiccant (silica gel)-lined finite flat plates and in channels. The problem is treated as conjugate flow, heat, and mass transfer, and solved by using a finite control-volume method. The effects of the plate thickness ($3 \le b \le 7$ mm), the Reynolds number ($333 \le \mathrm{Re} \le 3{,}333$), and the turbulence intensity ($1 \le TI \le 10\%$) on the dehumidification process are investigated. The results show that increasing the desiccant plate thickness decreases the heat and mass transfer coefficients by 25% and 22% at $t = 10$ s and $x = 0.11$ m, respectively, in comparison to a thin plate. Mass transport rates increase with Re, e.g., at $t = 20$ s, W_{ave} increases by 50% as Re is increased 10-fold from 333 to 3,333. Turbulent flow in channel desiccants increases the rate of dehumidification, e.g., an increase in Re from 600 (laminar) to 6,000 (turbulent) results in an increase in W_{ave} by 22% at $t = 20$ s. Also, increasing the turbulence intensity from 1% to 10% increase W_{ave} by 7%.

1. INTRODUCTION

This study develops more rigorous models and their numerical analysis for solid-bed desiccant systems used for gas dehumidification, so that the basic understanding of the process is advanced and ways for improving overall performance of such systems may be found more effectively. The models and numerical analyses found in the literature are nonconjugate, typically assuming that the desiccant bed is thin enough to ignore the heat and mass transfer in the desiccant (silica gel) bed, and applying the adsorptive properties of the desiccant as boundary conditions. A conjugate-transient two-dimensional numerical solution for humid transient laminar and turbulent air flow fields over desiccant-lined finite flat plates and inside channels, including the associated heat and mass transfer phenomena, is conducted here.

Received 30 January 2004; accepted 7 May 2004.

The first author is grateful for the financial support of his graduate studies by his employer, The General Organization of Technical Education and Vocational Training of Saudi Arabia, the Saudi Arabian Cultural Mission in Washington, DC.

The current address of Hassan Al-Sharqawi is Medina College of Technology, P.O. Box 1593, Medina, Saudi Arabia.

Address correspondence to Noam Lior, Department of Mechanical Engineering and Applied Mechanics, University of Pennsylvania, 111 Towne Building D3, 220 South 33rd street, Philadelphia, PA 19104-6315, USA. E-mail: lior@seas.upenn.edu

NOMENCLATURE

b	thickness of silica gel bed, m	u	x component of velocity, m/s
c	specific heat, kJ/kg K	$\overline{u}$	x component of mean velocity, m/s
C	water vapor concentration [=(kg water)/(kg mixture)]	v	y component of velocity, m/s
		$\overline{v}$	y component of mean velocity, m/s
D	water vapor diffusivity in air, m^2/s	W	water content, kg/kg
h	practical height, m	α	thermal diffusivity, m^2/s
h	channel width, m	ε	dissipation
h_q	heat transfer coefficient, $[=q/(T-T_\infty)]$ kW/m^2 °C	ν	kinematics viscosity, m^2/s
		ρ	density, kg/m^3
h_m	mass transfer conductance, $[=j/(C-C_\infty)]$ kg/m^2 s	σ	porosity
		τ	shear stress
H_l	sorption heat, kJ/kg	Φ	air humidity ratio in bulk stream [=(kg of vapor)/(kg of air)]
j	mass flux, kg/m^2 s		
K	kinetic energy		
L	length of silica gel bed, m	**Subscripts**	
m'''	water absorption rate into silica gel, kg/s m^3	ave	average
		b	bed
Pr	Prandtl number	f	fluid (i.e., air)
q	heat flux, kW/m^2	o	initial value
Sc	Schmidt number	s	silica gel
t	time, s	t	turbulent
T	temperature, °C	w	wall, i.e., the silica gel bed
TI	turbulent intensity	∞	free-stream conditions

The solid desiccant model developed and presented in this work is based on assuming heat conduction and mass diffusion through it, without going to the detailed flow and its associated transport through the pores of the desiccant. The first author modified this heat and mass transport model in the solid desiccant by posing and solving for the flow through the porous desiccant and the associated convective heat and mass transfer [1]. This more detailed modeling allowed better insight into the desiccation and regeneration processes, although the computation is much more time-consuming yet the overall results for the system and conditions considered in this article are very similar to those presented here.

Some of the most relevant past studies of this problem are by Fujii and Lior [2], who solved numerically the conjugate-transient two-dimensional heat and mass transfer problem with a steady laminar air stream passing over thick silica gel bed, and those by Pesaran and Mills [3, 4] and Kafui [5], who treated this problem theoretically and experimentally. In their theoretical work, their model and numerical analysis were non-conjugate. Pesaran and Mills [3] assumed uniform temperatures in the desiccant bed at any time, and Kafui [5] advanced the state of the art by allowing the desiccant temperature, $Tr(r, t)$, and water content, $W(r, t)$, to change both temporally and spatially.

More recently, Niu and Zhang [6] solved numerically the conjugate-transient two-dimensional heat and mass transfer in a laminar flow silica gel-lined channel, which is a cell in a desiccant wheel, to investigate the effects of the channel wall thickness on the optimal rotary speed of such wheels. They considered both the heat and the moisture resistance in both the axial and the thickness directions in the silica gel. Foss et al. [7] and Yong and Sumathy [8] studied heat and mass transfer in adsorbing beds, the former in paper sheets and the latter in a cylindrical

axisymmetric adsorber, but neither studied the conjugate problem of humid gas flow across a solid desiccant presented in this article.

In this article we address (1) a transient-laminar air stream passing over a flat desiccant bed 3–7 mm thick, and free-stream velocities of 0.1 to 1 m/s, (2) a transient-laminar and turbulent air stream in channels of 0.01–0.05 m width in which their internal walls are lined with desiccant; in the turbulent case, the problem was solved for turbulent intensities of 1–10%. The primary advancements of the model presented in this article are the conjugate approach, and the coupling of the transient flow and heat and mass transfer.

2. MODEL CONFIGURATION

The physical system considered (Figures 1 and 2) is a flat silica gel-packed desiccant bed of length L with a uniform air stream passing over it in parallel. Figure 1 shows the extended computational domain of the flat bed along the x direction, where h is the practical height in the y direction, L is the bed length, and b is the bed thickness. The extended domain up- and downstream of the bed was generated to allow correct numerical solution of the flow field.

3. GOVERNING EQUATIONS

3.1. Assumptions

Two-dimensional domain.
Laminar flow.
Transient velocity, temperature, and concentration fields.
Constant properties, since their variations with temperature in our temperature range of interest are very small. For example, in our study the temperature changes by about 4°C, with a corresponding air specific heat change of only about 0.4%.
No-slip boundary condition at the desiccant surface.
Adiabatic desiccant bottom surface.
Continuity of heat and mass flux and temperature at the fluid–solid interface.
No heat or mass flux in the silica gel bed in the x direction.

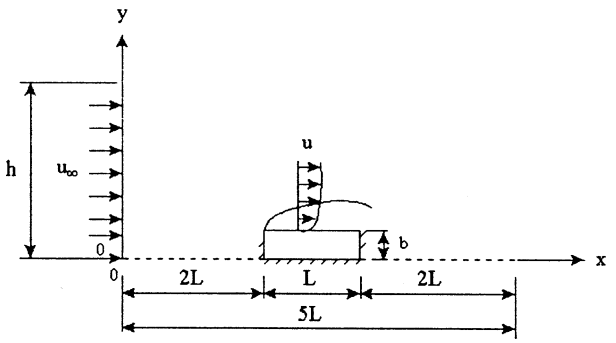

Figure 1. The domain extended along the flow (x) direction.

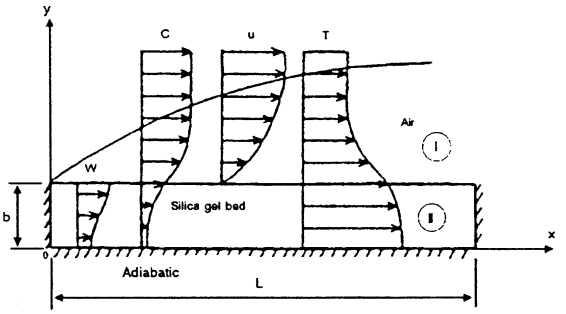

Figure 2. The physical model configuration for the flat desiccant bed located in the extended computational domain.

3.2. Fundamental Equations

3.2.1. Region I (Figure 2). For laminar air and water vapor flow, these are the continuity, x and y momentum, energy, and mass diffusion equations as shown in [2], and will not be repeated here
For turbulent air and water vapor flow,
Continuity:

$$\frac{\partial \rho}{\partial t} + \frac{\partial(\rho \overline{u})}{\partial x} + \frac{\partial(\rho \overline{v})}{\partial y} = 0 \tag{1}$$

x-Momentum:

$$\frac{\partial \overline{u}}{\partial t} + \overline{u}\frac{\partial \overline{u}}{\partial x} + \overline{v}\frac{\partial \overline{u}}{\partial y} = -\frac{1}{\rho}\frac{\partial \overline{p}}{\partial x} + \frac{\partial}{\partial x}\left[(\nu + \nu_t)\frac{\partial \overline{u}}{\partial x}\right] + \frac{\partial}{\partial y}\left[(\nu + \nu_t)\frac{\partial \overline{u}}{\partial y}\right] + \left\{\frac{\partial}{\partial x}\left[(\nu + \nu_t)\frac{\partial \overline{u}}{\partial x}\right] + \frac{\partial}{\partial y}\left[(\nu + \nu_t)\frac{\partial v}{\partial x}\right]\right\} \tag{2}$$

y-Momentum:

$$\frac{\partial \overline{v}}{\partial t} + \overline{u}\frac{\partial \overline{v}}{\partial x} + \overline{v}\frac{\partial \overline{v}}{\partial y} = -\frac{1}{\rho}\frac{\partial \overline{p}}{\partial y} + \frac{\partial}{\partial x}\left[(\nu + \nu_t)\frac{\partial \overline{v}}{\partial x}\right] + \frac{\partial}{\partial y}\left[(\nu + \nu_t)\frac{\partial \overline{v}}{\partial y}\right] + \left\{\frac{\partial}{\partial x}\left[(\nu + \nu_t)\frac{\partial \overline{u}}{\partial y}\right] + \frac{\partial}{\partial y}\left[(\nu + \nu_t)\frac{\partial \overline{v}}{\partial y}\right]\right\} \tag{3}$$

Kinetic energy (K):

$$\frac{\partial K}{\partial t} + \overline{u}\frac{\partial K}{\partial x} + \overline{v}\frac{\partial K}{\partial y} = \frac{\partial}{\partial x}\left(\frac{\nu_t}{pr^k}\frac{\partial K}{\partial x}\right) + \frac{\partial}{\partial y}\left(\frac{\nu_t}{pr^k}\frac{\partial K}{\partial y}\right) + \nu_t\left[2\left(\frac{\partial \overline{u}}{\partial x}\right)^2 + 2\left(\frac{\partial \overline{v}}{\partial y}\right)^2 + \left(\frac{\partial \overline{u}}{\partial y} + \frac{\partial \overline{v}}{\partial x}\right)^2\right] - \varepsilon \tag{4}$$

Dissipation (ε):

$$\frac{\partial \varepsilon}{\partial t}+\overline{u}\frac{\partial \varepsilon}{\partial x}+\overline{v}\frac{\partial \varepsilon}{\partial y}=\frac{\partial}{\partial x}\left(\frac{\nu_t}{pr^{\varepsilon}}\frac{\partial \varepsilon}{\partial x}\right)+\frac{\partial}{\partial y}\left(\frac{\nu_t}{pr^{\varepsilon}}\frac{\partial \varepsilon}{\partial y}\right)$$
$$+C_1\nu_t\frac{\varepsilon}{K}\left[2\left(\frac{\partial \overline{u}}{\partial x}\right)^2+2\left(\frac{\partial \overline{v}}{\partial y}\right)^2+\left(\frac{\partial \overline{u}}{\partial y}+\frac{\partial \overline{v}}{\partial x}\right)^2\right]-C_2\frac{\varepsilon^2}{K} \tag{5}$$

Energy:

$$\frac{\partial \overline{T}}{\partial t}+\overline{u}\frac{\partial \overline{T}}{\partial x}+\overline{v}\frac{\partial \overline{T}}{\partial y}=\frac{\partial}{\partial x}\left[\left(\frac{\nu}{pr}+\frac{\nu_t}{pr_t}\right)\frac{\partial \overline{T}}{\partial x}\right]+\frac{\partial}{\partial y}\left[\left(\frac{\nu}{pr}+\frac{\nu_t}{pr_t}\right)\frac{\partial \overline{T}}{\partial y}\right] \tag{6}$$

Mass diffusion:

$$\frac{\partial \overline{C}}{\partial t}+\overline{u}\frac{\partial \overline{C}}{\partial x}+\overline{v}\frac{\partial \overline{C}}{\partial y}=\frac{\partial}{\partial x}\left[\left(\frac{\nu}{sc}+\frac{\nu_t}{sc_t}\right)\frac{\partial \overline{C}}{\partial x}\right]+\frac{\partial}{\partial y}\left[\left(\frac{\nu}{sc}+\frac{\nu_t}{sc_t}\right)\frac{\partial \overline{C}}{\partial y}\right] \tag{7}$$

where ν_t is the turbulent eddy diffusivity,

$$\nu_t=\frac{C_\mu K^2}{\varepsilon} \tag{8}$$

The empirical constants in the k–ε model relation have the following values according to [9]: $C_\mu=0.09$, $C_1=1.44$, $C_2=1.92$, $\mathrm{Pr}^k=1.0$, $\mathrm{Pr}^{\varepsilon}=1.3$, $\mathrm{Pr}_t=0.9$, where Pr^k and $\mathrm{Pr}^{\varepsilon}$ are effective Prandtl numbers and Pr_t is turbulent Prandtl number.

3.2.2. Region II: The silica gel bed [2]

Energy:

$$\frac{\partial T}{\partial t}=\alpha_w\left(\frac{\partial^2 T}{\partial x^2}+\frac{\partial^2 T}{\partial y^2}\right)+\frac{H_l m'''}{c_w\rho_w} \tag{9}$$

$c_w\rho_w$ is the thermal capacity of the desiccant,

$$c_w\rho_w=\sigma c_f\rho_f+(1-\sigma)c_s\rho_s \tag{10}$$

Water vapor diffusion:

$$\sigma\frac{\partial C}{\partial t}=D_w\left(\frac{\partial^2 C}{\partial x^2}+\frac{\partial^2 C}{\partial y^2}\right)-\frac{m'''}{\rho_f} \tag{11}$$

The water adsorption rate in the silica gel is expressed as

$$m'''=(1-\sigma)\rho_s\frac{\partial W}{\partial t} \tag{12}$$

The relationship between the water content in silica gel and water vapor concentration at the local equilibrium, $W = f(C,T)$, is an empirical relation, different for each desiccant. From [10], the relation used for silica gel is

$$\Phi = \frac{10^s C}{0.622 + C} \tag{13}$$

where

$$(-\Phi - 9.31077 + 0.001717651 T_w^2) + (478.0868 + 9.18715 \times 10^{-5} T_1^3) w - 1417.118 w^2 + 2094.818 w^3 = 0 \tag{14}$$

and

$$s = 4.21429 - \frac{7.5 T_w}{237.3 + T_w} \tag{15}$$

where T_w is the silica gel temperature (°C) and T_1 is the ambient air temperature (°C).

Equations (1)–(12) are used to solve for the unknown parameters u, v, T, and C in the air flow (region I), and for T, C, w, and m''' in the silica gel (region II).

3.3. Boundary Conditions

3.3.1. General. Insulated bottom surface, continuity of heat and mass fluxes, no heat or mass flux in silica gel bed in the x direction, and no slip at the walls were applied as in [2].

The upstream conditions are

$$u(0, y, t) = u_\infty \tag{16}$$

$$v(0, y, t) = 0 \tag{17}$$

$$T(0, y, t) = T_\infty \tag{18}$$

$$C(0, y, t) = C_\infty \tag{19}$$

The downstream conditions are

$$\frac{\partial u(x = 5L, y, t)}{\partial x} = \frac{\partial v(x = 5L, y, t)}{\partial x} = 0 \tag{20}$$

$$\frac{\partial T(x = 5L, y, t)}{\partial x} = \frac{\partial C(x = 5L, y, t)}{\partial x} = 0 \tag{21}$$

The top condition for the flat-plate desiccant bed is

$$\frac{\partial v(0 \le x \le 5L, y = h, t)}{\partial y} = 0 \tag{22}$$

$$u(0 \le x \le 5L, y = h, t) = u_\infty \tag{23}$$

The top condition for the channel desiccant is

$$\frac{\partial u(0 \le x \le 5L, y = h, t)}{\partial y} = \frac{\partial T(0 \le x \le 5L, y = h, t)}{\partial y}$$

$$= \frac{\partial C(0 \le x \le 5L, y = h, t)}{\partial y} = 0 \tag{24}$$

$$\frac{\partial K(0 \le x \le 5L, y = h, t)}{\partial y} = \frac{\partial \varepsilon(0 \le x \le 5L, y = h, t)}{\partial y} = 0 \tag{25}$$

$$v(0 \le x \le 5L, y = h, t) = 0 \tag{26}$$

The bottom condition for the channel desiccant is

$$\frac{\partial u(0 \le x \le 5L, y = 0, t)}{\partial y} = \frac{\partial T(0 \le x \le 5L, y = 0, t)}{\partial y} =$$

$$\frac{\partial C(0 \le x \le 5L, y = 0, t)}{\partial y} = 0 \tag{27}$$

$$\frac{\partial K(0 \le x \le 5L, y = 0, t)}{\partial y} = \frac{\partial \varepsilon(0 \le x \le 5L, y = 0, t)}{\partial y} = 0 \tag{28}$$

$$v(0 \le x \le 5L, y = 0, t) = 0 \tag{29}$$

3.3.2. Boundary condition in the near-wall region for turbulent flow [9, 11]. From the momentum equation,

$$u^+ = y^+ \qquad y^+ \le 10 \tag{30}$$

$$u^+ = 2.5 \ln 9y^+ \qquad y^+ \ge 10 \tag{31}$$

where

$$u^+ = \frac{u_\infty}{u^*} \tag{32}$$

$$y^+ = \frac{yu^*}{v} \tag{33}$$

$$u^* = \sqrt{\frac{\tau_w}{\rho}} \tag{34}$$

The near-wall temperature and concentration [11] are

$$T^* = \frac{\alpha q_w}{ku^*} \tag{35}$$

$$T^* = \frac{T_w - T}{T^*} \tag{36}$$

From the energy equation,

$$T^+ = \mathrm{Pr}\, y^+ \qquad y^+ \leq 10 \tag{37}$$

$$T^+ = 2.5\,\mathrm{Pr}_t\, \ln 9y^+ \qquad y^+ \geq 10 \tag{38}$$

where Pr_t is the turbulent Prandtl number.

Analogous to the near-wall temperature, the concentration is

$$C^+ = \mathrm{Sc}\, y^+ \qquad y^+ \leq 10 \tag{39}$$

$$C^+ = 2.5\,\mathrm{Sc}_t\, \ln 9y^+ \qquad y^+ \geq 10 \tag{40}$$

where Sc_t is turbulent Schmidt number.

3.4. Initial Conditions

$$u(x, y, 0) = u_\infty \tag{41}$$

$$T(x, y, 0) = T_\infty \tag{42}$$

$$C(x, y, 0) = C_\infty \tag{43}$$

$$C(2L < x < 3L, y \leq b, 0) = C_w \tag{44}$$

$$W(2L < x < 3L, y \leq b, 0) = f(C_w, T_\infty) \tag{45}$$

4. METHOD OF SOLUTION

The continuity and momentum equations were solved by the SIMPLER (Semi-Implicit Method for Pressure-Linked Equation Revised) algorithm control-volume method [12]. Grid independence and convergence were examined and ensured for a grid size of $250 \times 150(x, y)$, where the computational relative error was an acceptable 10^{-4}. The solution converged at each step after about 46 iterations (depending on the mesh size), so 120–250 iterations were made for safety.

5. RESULTS AND DISCUSSION

5.1. Laminar Flow Fields over Desiccant Finite Flat Plate

5.1.1. Reduction of velocity overshoots. An interesting phenomenon was encountered during the flow computations over a finite-length plate modeled as shown in Figure 1: when the uniform free-stream velocity was applied at the leading

edge, the results showed a 12% velocity overshoot (over the free-stream velocity) near the boundary-layer edge. While overshoots were measured [13] in laminar flow ($20 < \mathrm{Re} < 3{,}000$), and computationally predicted in [14] for $10^2 < \mathrm{Re} < 10^5$, they occurred only at the trailing edge and the near wake, and not over the plate as our initial results showed. Several different approaches were undertaken to examine whether this velocity overshoot is just a computational artifact as it seemed to be, and several methods, including grid refinement and extension of the computational domain farther in the y direction to allow a more gradual approach to the boundary conditions at the top of the domain were used, but it remained there. The overshoot has been reduced finally by extending the computational domain by a length $2L$ both upstream and downstream of the plate along the x direction. It is noteworthy that the overshoot decreases somewhat as the Reynolds number (Re_L) increased, even without having to extend the computational domain along x, falling below about 3% for $\mathrm{Re} \approx 27{,}000$ ($u_\infty = 8\ \mathrm{m/s}$).

5.1.2. Velocity field and its gradients. The need to predict the correct velocity field is emphasized by the fact that here we need to predict correctly the heat and mass transfer rates, as well as the pressure drop, all of which are strongly affected by the velocity gradient at the desiccant surface. To demonstrates the importance of correct prediction of the velocity field, the velocity gradient $\partial u / \partial y$ at the plate trailing edge and $y = b$, computed without extending the computational domain, is about 72% smaller than that computed for the extended domain.

Figures 3*a*–3*d* show the u and v velocity profiles at different positions along the plate for three different bed thicknesses (extended domain computation). As expected, u decelerates upstream of the plate leading edge due to the pressure rise brought on by the stagnation point at the frontal area of the bed. The deceleration in the boundary layer progresses along the plate, and even flow reversal is reached for thicker plates. A wake region follows the downstream edge. The front and rear edges also exhibit stronger mixing, with, as will be shown below, higher heat and mass transfer rates. As also expected, the flow velocity and gradient changes become decreasingly pronounced as the plate thickness is increased.

The normal velocity v is seen (Figures. 3*c* and 3*d*) to accelerate in the vertical direction upstream of the leading edge, and exhibits a direction reversal (toward the plate) at some point along the plate surface, and in regions of the wake. The flow deceleration rate increases as the bed thickness increases.

Figures 4*a* and 4*b* show the velocity distributions as a function of y at different x positions, with similar conclusions. It can be seen that the velocity gradient at the desiccant surface decreases along the plate. Some backflow (negative velocity) starts developing when the bed thickness is increased to 7.26 mm, and it increases to about 10% when the bed thickness is 9.29 mm (Figure 4*b*). The backflow and flow disturbance are almost absent up to bed thickness of about 5 mm, but they develop very quickly beyond this thickness.

5.2. Heat and Mass Transfer Results

5.2.1. Validation of the heat and mass transfer results. Our analysis of the conjugate-transient two-dimensional heat and mass transfer problem between

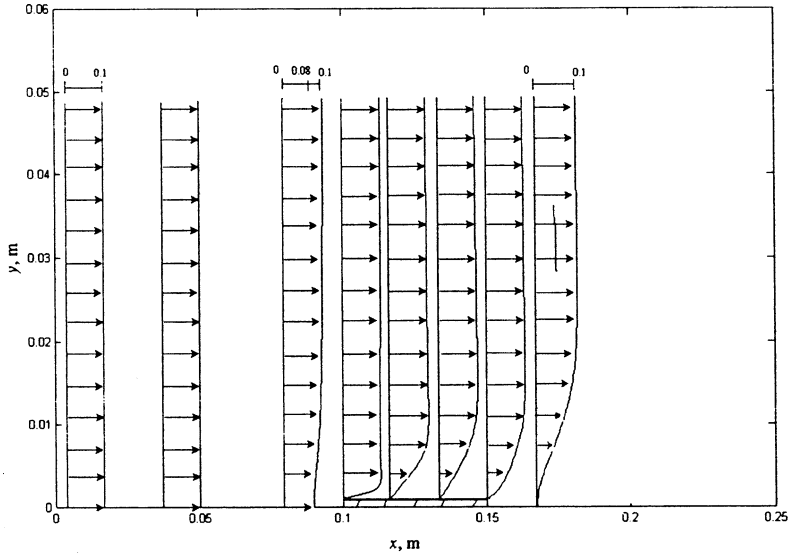

a. (u velocity) $u_\infty = 0.1$ m/s, $Re_L = 333$, $b = 0.00118$ m

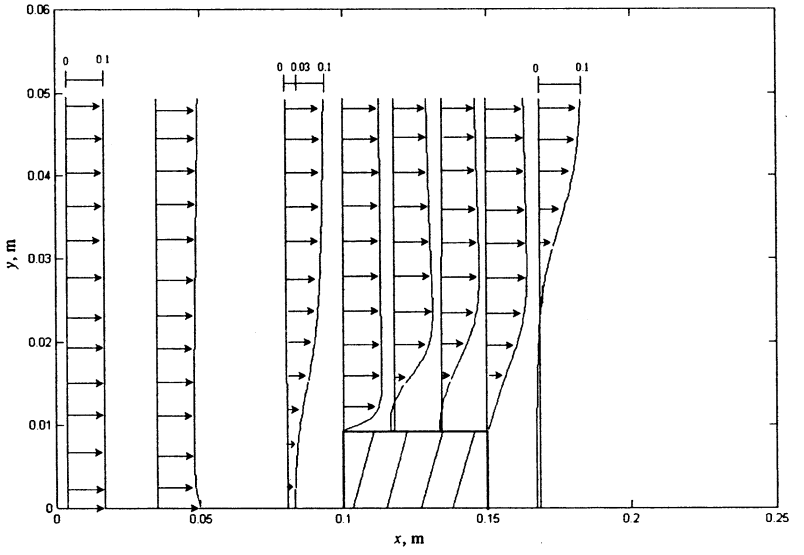

b. (u velocity) $u_\infty = 0.1$ m/s, $Re_L = 333$, $b = 0.00118$ m

Figure 3. The u and v velocity profiles at different x positions.

a silica gel bed and transient humid laminar air stream are compared with the only appropriate results that we could find, Pesaran's theoretical and experimental models [3, Run 1] for the system and conditions he used. His theoretical model is nonconjugate, justified by him by the statement that the silica gel bed is thin enough to consider the internal temperature and concentration constant and/or assigning empirical heat and mass transfer coefficients at the desiccant-air interface without

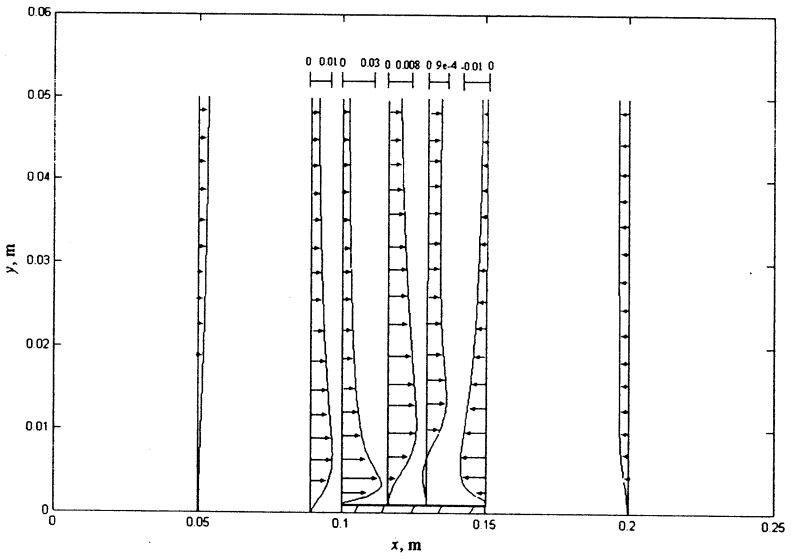

c. (v velocity) $u_\infty = 0.1$ m/s, $Re_L = 333$, $b = 0.00118$ m

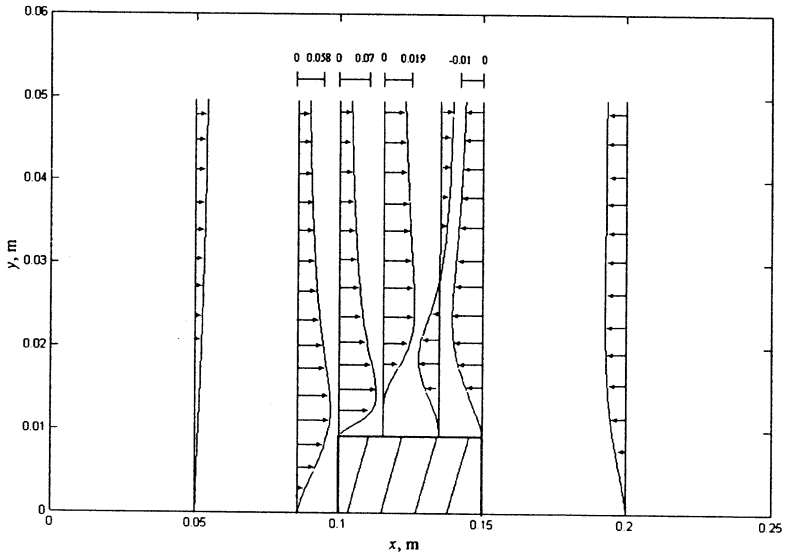

d. (v velocity) $u_\infty = 0.1$ m/s, $Re_L = 333$, $b = 0.00929$ m

Figure 3. Continued.

including the interfacial region in the numerical solution of the flow and desiccant bed equations. Figures 5*a* and 5*b*, showing the predictions of our conjugate and non-conjugate models of the outlet temperature and concentration as a function of time, demonstrate close agreement between our conjugate model solution, within 1.5°C for the temperature and 8% for the concentration, and Pesaran's results (which were also validated by him experimentally). Considering the fact that under these

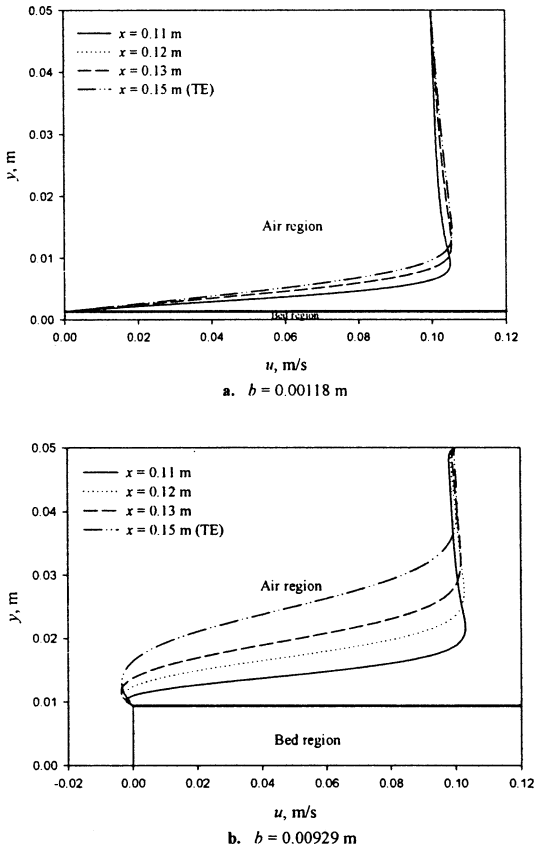

Figure 4. The u velocity profiles over the bed at four x locations, for different bed thickness b: $u_\infty = 0.1$ m/s, $\mathrm{Re}_L = 333$, $L = 0.05$ m, $h = 0.05$ m.

conditions the difference between the results of the nonconjugate and conjugate models is only about 1.7°C for the temperature and 7% for the concentration, and considering the magnitude of the experimental error, the agreement between our results and the experiments is rather good.

5.2.2. Laminar flow over flat desiccant bed. Figures 6*a* and 6*b* show the isotherms (°C) and constant concentration line (kg/kg) contours, respectively, in both the humid air and the desiccant bed regions. Both the isotherms and the constant concentration contours between the leading and trailing edges of the bed display the development of the thermal and the concentration boundary layer over the bed as y increases. In the bed, the temperature increases with y. Along the flow direction (x) it can be seen that the concentration of water in the air decreases first rapidly, then stabilizes, and finally increases slightly near the downstream edge; the opposite takes place in the desiccant. These phenomena are explained in more detail below, but basically reflect the initial rapid air dehumidification because of both the initial relative dryness of the bed and high velocity gradients (convection rates) at low values of x, with gradual move toward saturation.

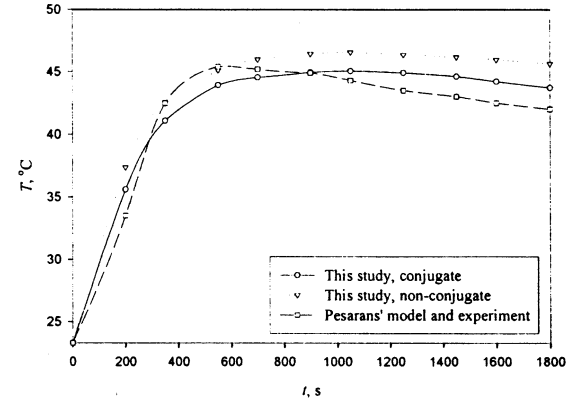

a. Outlet temperature

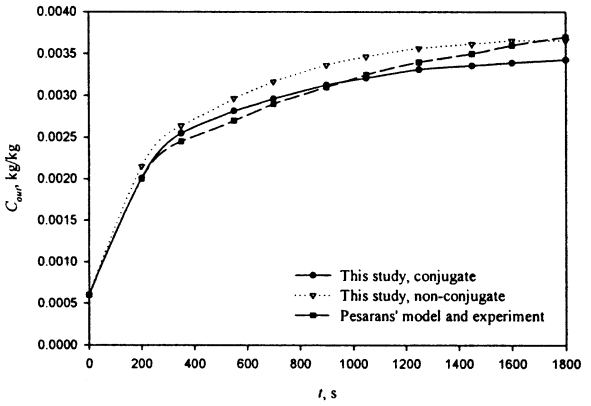

b. Outlet concentration

Figure 5. Comparison of outlet temperature and concentration for this study with the theoretical and experimental models of [2,3], for adsorption: $u_\infty = 0.21$ m/s, $T_\infty = 23.3°C$, $C_{in} = 0.01$ kg/kg, $W_o = 0.0417$ kg/kg, $L = 0.0775$ m, $D_f = 2.79 \times 10^{-5}$ m^2/s, $\alpha_s = 8.8 \times 10^{-5}$ m^2/s, $\rho_f = 1.2$ kg/m^3, $H_l = 2550$ kJ/kg.

Figures 7*a*–7*d* shows the time dependence at $x = 0.11$ m ($0.2L$ from the leading edge of the plate) of the desiccant surface water concentration, surface temperature, as well as the overall average water content and adsorption rate for three different bed thicknesses. As expected, all of these quantities increase more rapidly at first, and then increase at a slower rate as the bed becomes increasingly water-laden and thus cannot take up vapor as rapidly. The time step used in these computations is 0.1 s. The convective heat and mass transfer coefficients are related to the velocity gradient $\partial u/\partial y$ through the temperature and concentration gradients in the y direction, and follow their transient behavior discussed in Section 5.1.2. Starting with the high initial value, the convective heat and mass transfer coefficients decrease until 0.4 s, and then grow monotonically and asymptotically. Because of the local equilibrium relations, the water content exhibits similar behavior to that of the temperature and concentration. An initial

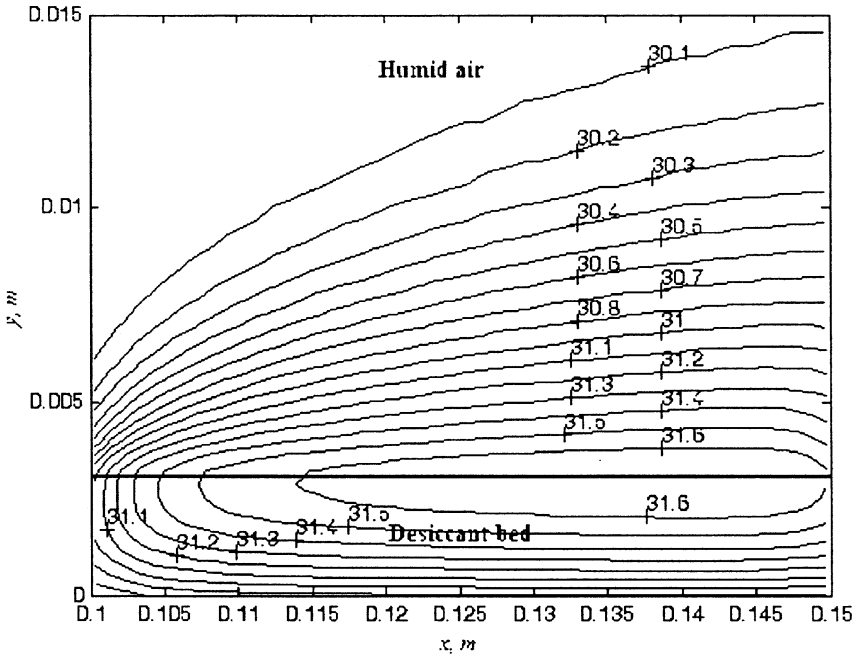

a. Isotherms (°C)

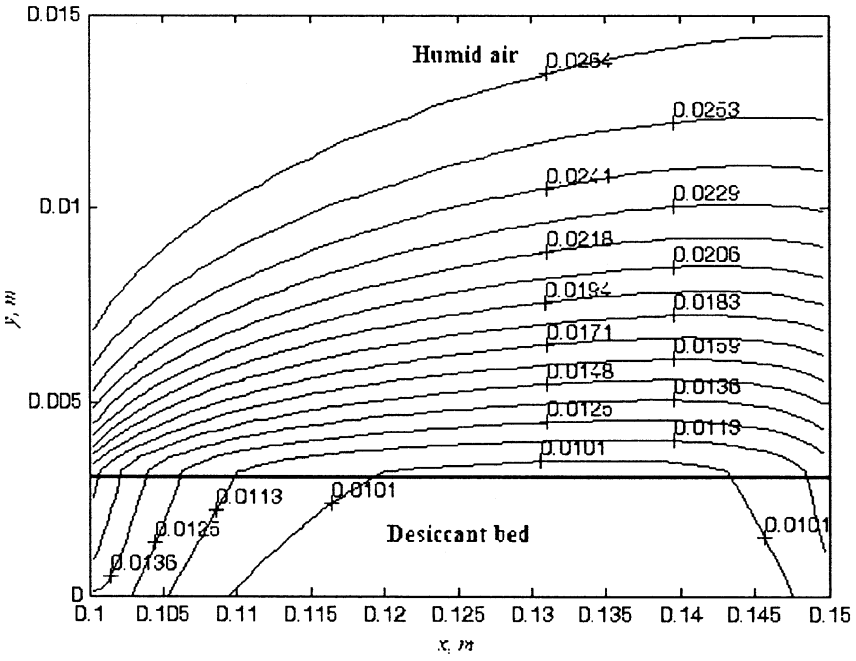

b. Constant concentration lines (kg/kg)

Figure 6. Isotherms and constant concentration lines contours in the humid air and the desiccant bed regions: $u_\infty = 0.1$ m/s, $\mathrm{Re}_L = 333$, $T_\infty = 30°\mathrm{C}$, $C_\infty = 0.0276$ kg/kg, $C_b = 0.0075$ kg/kg, $W_o = 0.1$ kg/kg, $b = 0.00321$ m, $L = 0.05$ m, $h = 0.05$ m, $\sigma = 0.1$, $t = 20$ s.

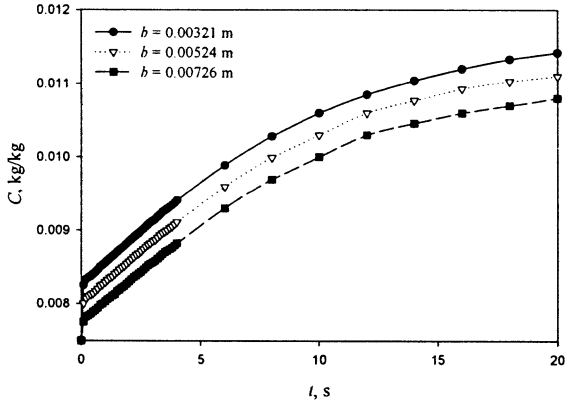

a. Desiccant surface water concentration, $x = 0.11$ m

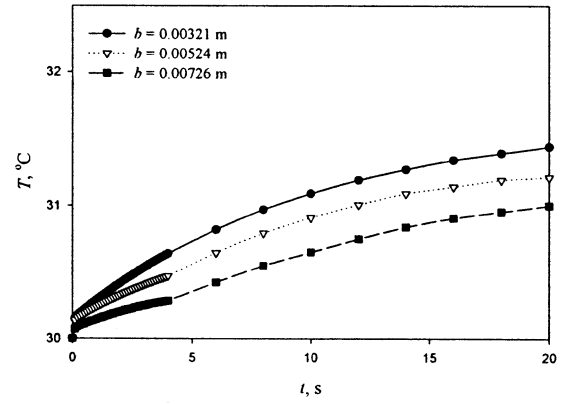

b. Desiccant surface temperature, $x = 0.11$ m

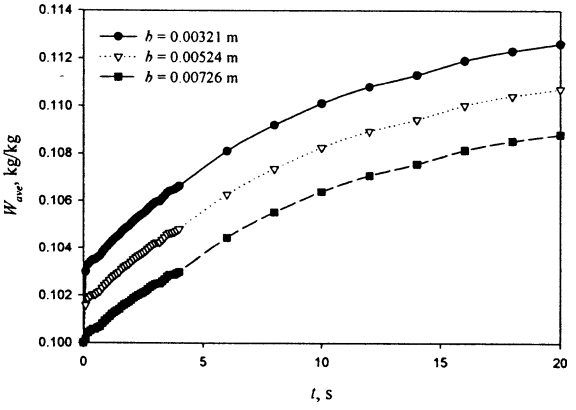

c. Desiccant overall average water content

Figure 7. Time dependence of desiccant surface ($y = b$): (*a*) water concentration, (*b*) surface temperature, (*c*) overall average water content, and (*d*) overall average adsorption rate for different bed thicknesses, $u_\infty = 0.1$ m/s, $\mathrm{Re}_L = 333$, $T_\infty = 30°\mathrm{C}$, $C_\infty = 0.0276$ kg/kg, $C_b = 0.0075$ kg/kg, $W_o = 0.1$ kg/kg, $L = 0.05$ m, $h = 0.05$ m, $\sigma = 0.1$.

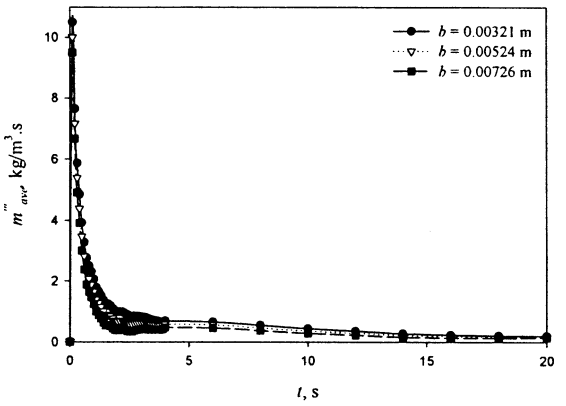

d. Desiccant overall average water adsorption rate

Figure 7. Continued.

rise in the water adsorption rate occurs due to the rapid rise in the water content. The magnitudes of the surface water concentration and the surface temperature as well as the overall average water content and adsorption rate decrease as the bed thickness increases (at 1.3%/mm, 0.11°C/mm, 0.82%/mm, and 7.44%/mm, respectively), determined at 20 s (for all variables in Figure 7), due to the reduction in the u velocity gradient in the y direction near the air–desiccant interface (Figure 3) as the bed thickness increases, which causes the reduction in the transport coefficient (see Figure 9).

The equations used in this model are valid as long as the desiccant has not reached a state beyond saturation. Silica gel reaches saturation when the water content is 38% at 100% ϕ (relative humidity), which is obtained at $T = 65.7$°C and according to the silica gel isotherm [Eq. (14)]. The analysis shows that the average maximal water content in this study is reached at $t = 20$ s and $b = 3.21$ mm, and amounts to about 11.2%, as shown in Figure 7*c*, indicating that the silica gel did not reach saturation state, and thus water condensation effects do not need to be considered in the model.

Figures 8*a* and 8*b* show the water content change with x at the desiccant surface ($y = 0.00321$ m), and with the y direction at two x positions, respectively. As seen in Figure 8*a*, the surface water content at the bed leading edge ($x = 0.1$ m) is relatively large because $\partial u/\partial y$ near the air–desiccant interface is large (see Figure 9*b*). The surface water content decays with x due to the corresponding reduction in $\partial u/\partial y$, which causes the reduction in mass transport coefficient (see Figure 9*b*). It is noteworthy here that the surface water content increases slightly toward the end of the plate ($x = 0.148$–0.15 m), in the vicinity of the trailing edge ($x = 0.15$ m), due to the increase in the local mass transport coefficient (see Figure 9*b*). The water content inside the desiccant is seen in Figure 8*b* to decrease from the bed surface down toward its bottom, and the water penetration is to lower depth at lower values of x, as expected.

Figures 9*a* and 9*b* show the local heat and mass transfer coefficients along the desiccant bed for three different bed thicknesses. The local heat and mass transfer

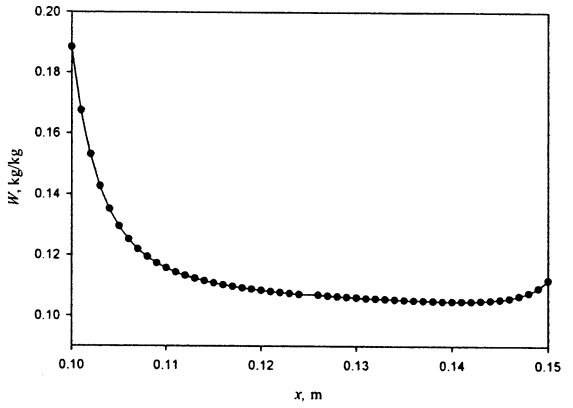

a. Water content as a function of x, y = 0.00321 m

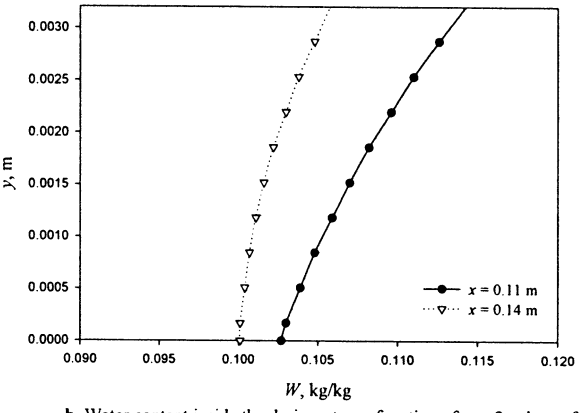

b. Water content inside the desiccant as a function of y at 2 values of

Figure 8. Water content as functions of x and y at $t = 20$ s: $u_\infty = 0.1$ m/s, $\mathrm{Re}_L = 333$, $T_\infty = 30°\mathrm{C}$, $C_\infty = 0.0276$ kg/kg, $C_b = 0.0075$ kg/kg, $W_o = 0.1$ kg/kg, $b = 0.00321$ m, $L = 0.05$ m, $h = 0.05$ m, $\sigma = 0.1$.

coefficients are computed near the air–desiccant interface along x and at $y = 0.0035$ m, where the heat and mass transport is important. As seen in Figure 9, the heat and mass transfer coefficients at the beginning of the bed length at $x = 0.1$ m (leading edge) are relatively large because the u velocity gradient in the y direction near the air-desiccant interface is large (Figure 3). The heat and mass transfer coefficients decay as x increases, in concord with the change of $\partial u/\partial y$ (Figure 3). The magnitudes of the heat and mass transfer coefficient decrease with bed thickness (at 6.2%/mm and 7.3%/mm, respectively, at $x = 0.11$ m and $t = 20$ s for all variables), again due to the reduction $\partial u/\partial y$ near the bed–air interface as the bed thickness increases (Figure 3).

The effects of the Reynolds number at $x = 0.11$ m for one bed thickness ($b = 0.0032$ m) are shown in Figure 10. Mass transport rates increase with Re; for example, at $t = 20$ s, W_{ave} increases by 50% as Re is increased 10-fold, from 333 to 3,333, due to the increase in the convective heat and mass transfer coefficients at higher Reynolds numbers, since convection is the driving force here.

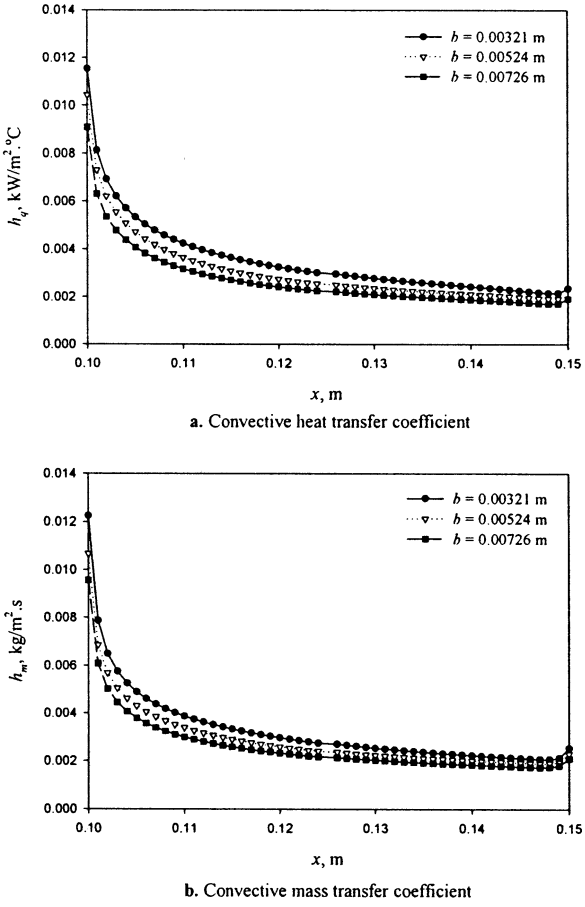

Figure 9. Convective heat and mass transfers coefficients along the desiccant bed for different bed thicknesses: $u_\infty = 0.1$ m/s, $\mathrm{Re}_L = 333$, $T_\infty = 30°\mathrm{C}$, $C_\infty = 0.0276$ kg/kg, $C_b = 0.0075$ kg/kg, $W_o = 0.1$ kg/kg, $L = 0.05$ m, $h = 0.05$ m, $\sigma = 0.1$, $t = 20$ s.

5.2.3. Dehumidification during laminar flow in channels. Here we investigate dehumidification in infinitely wide channel flows, where both channel walls are made of desiccant. As shown in Figure 11, increasing the channel height from 0.01 to 0.05 m reduces the desiccant surface concentration, surface temperature, W_{ave}, and, m'''_{ave} (at $t = 20$ s) by 10%, 0.9°C, 5% and 20%, respectively. This is due to the reduction in $\partial u/\partial y$ near the air–desiccant interface as the channel height increases, which causes a reduction in the transport coefficient.

Figure 12 shows a comparison of dehumidification over a flat-plate desiccant and in a desiccant channel. The average water content for flow in a channel is about 7% (at $t = 20$ s) higher than that over a flat bed, resulting from the fact that $\partial u/\partial y$ in the channel is 15% higher.

5.2.4. Dehumidification with turbulent flow in channels. It is expected that turbulent flow in channel desiccants would improve the rate of dehumidification,

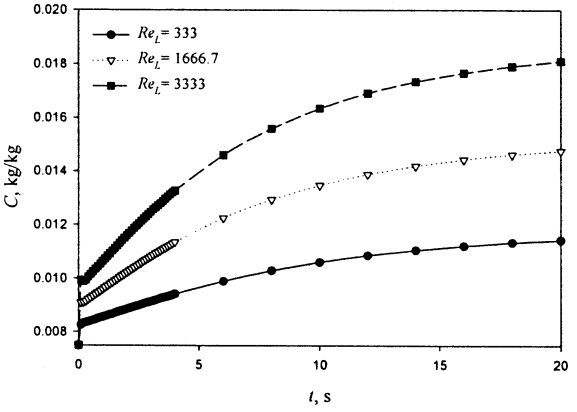

a. Desiccant surface water concentration, $x = 0.11$ m

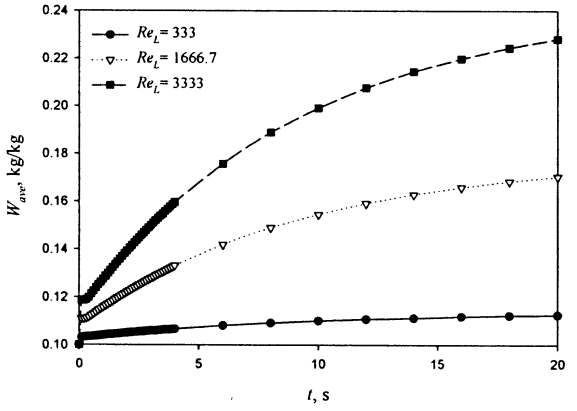

c. Desiccant overall average water content

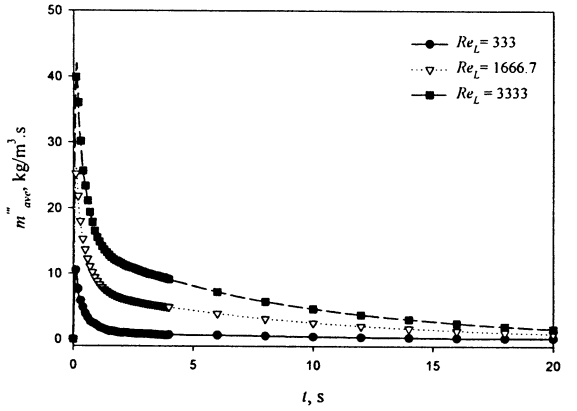

d. Desiccant overall average water adsorption rate

Figure 10. Time dependence of desiccant (*a*) surface ($y = b$) water concentration, (*b*) surface temperature, (*c*) average water content, and (*d*) average adsorption rate for different Reynolds numbers: $T_\infty = 30°C$, $C_\infty = 0.0276$ kg/kg, $C_b = 0.0075$ kg/kg, $W_o = 0.1$ kg/kg, $b = 0.00321$ m, $L = 0.05$ m, $h = 0.05$ m, $\sigma = 0.1$.

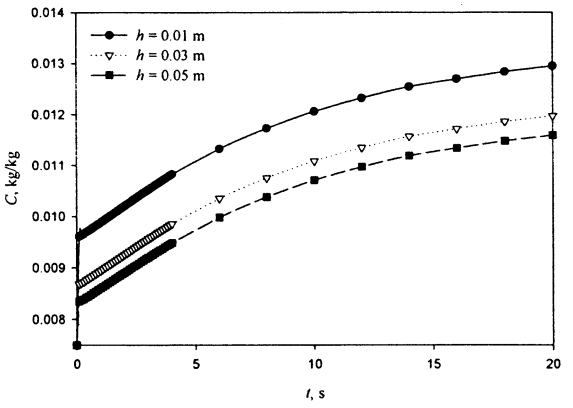

a. Desiccant surface water concentration, $x = 0.11$ m

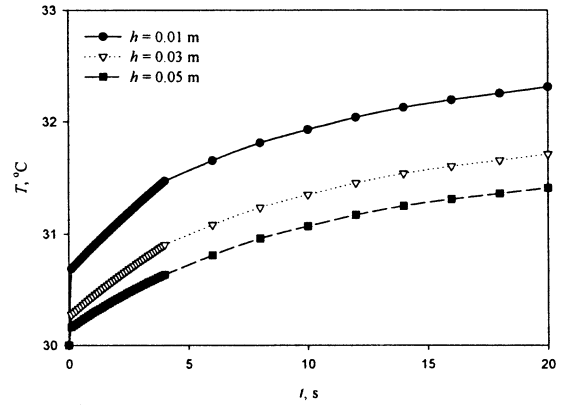

b. Desiccant surface temperature, $x = 0.11$ m

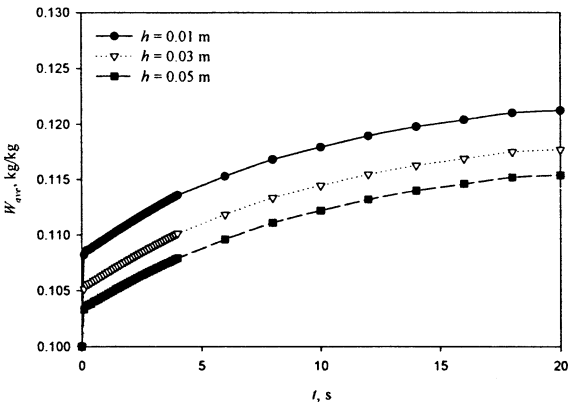

c. Desiccant overall average water content

Figure 11. Time dependence of desiccant surface ($y = b$) (*a*) water concentration, (*b*) surface temperature, (*c*) overall average water content, and (*d*) overall average water adsorption rate for different channel heights with 250 grid points in the x direction and 150 points in the y direction: $u_\infty = 0.1$ m/s, $T_\infty = 30°C$, $C_\infty = 0.0276$ kg/kg, $C_b = 0.0075$ kg/kg, $W_o = 0.1$ kg/kg, $b = 0.00321$ m, $L = 0.05$ m, $\sigma = 0.1$.

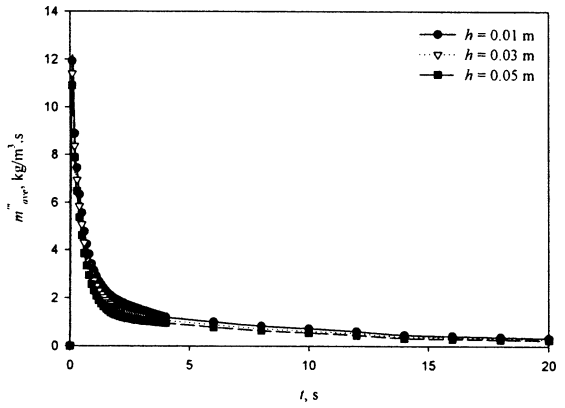

d. Desiccant overall average water adsorption rate

Figure 11. Continued.

and, as shown in Figure 13, increasing Re from 600 (laminar) to 6,000 (turbulent) increases W_{ave} by 22% at $t = 20$ s, and by 10% at $t = 2$ s.

The effect of the turbulence intensity (TI) is shown in Figure 14. As expected, W_{ave} and m'''_{ave} increase with the turbulence intensity (TI); for example, at t = 20 s by 7% and 20%, respectively, when the intensity is increased 10-fold, from 1% to 10%.

5.2.5. Summary of the heat and mass transfer results. A summary of the heat and mass transfer results of the adsorption processes for the parameters of interest is presented in Table 1. The percentage change in parameter is defined as

$$\% \text{ change in } \zeta = \frac{\zeta(\theta_L) - \zeta(\theta_S)}{\zeta(\theta_S)} \times 100 \tag{46}$$

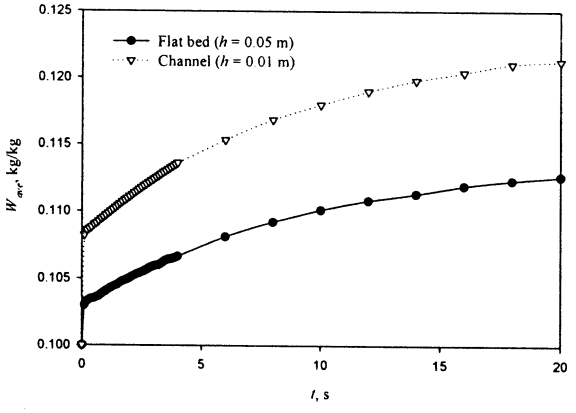

Figure 12. Time dependence of average water content in plate and channel desiccant beds, laminar flow: $u_\infty = 0.1$ m/s, (flat plate) $\text{Re}_L = 333$, (channel) $\text{Re} = 600$, $T_\infty = 30°\text{C}$, $C_\infty = 0.0276$ kg/kg, $C_b = 0.0075$ kg/kg, $W_o = 0.1$ kg/kg, $b = 0.00321$ m, $L = 0.05$ m, $\sigma = 0.1$.

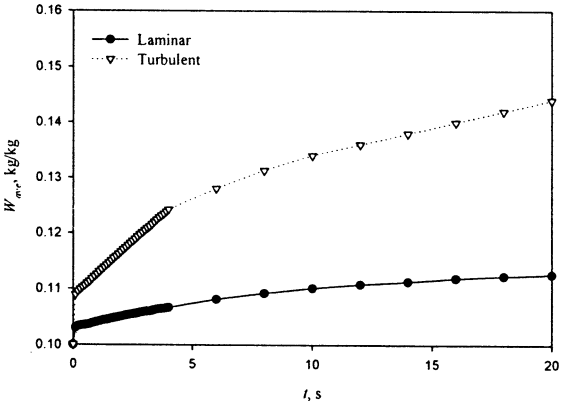

Figure 13. Time dependence of average water content in the desiccant for laminar and turbulent flows in channel: $u_\infty = 0.1$ m/s (laminar), $\mathrm{Re}_L = 600$, $u_\infty = 1$ m/s (turbulent, TI = 5%), $\mathrm{Re}_t = 6{,}000$, $T_\infty = 30°\mathrm{C}$, $C_\infty = 0.0276$ kg/kg, $C_b = 0.0075$ kg/kg, $W_o = 0.1$ kg/kg, $b = 0.00321$ m, $L = 0.05$ m, $h = 0.05$ m, $\sigma = 0.1$.

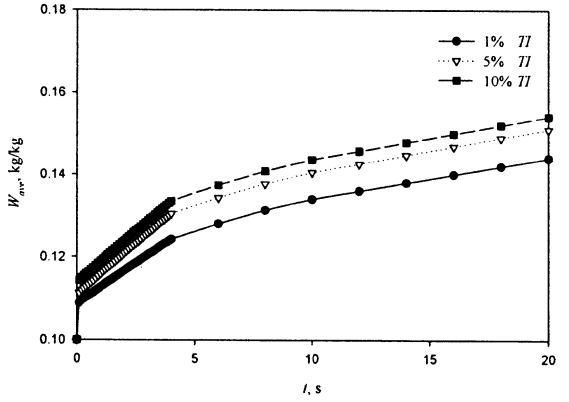

a. Desiccant overall average water content

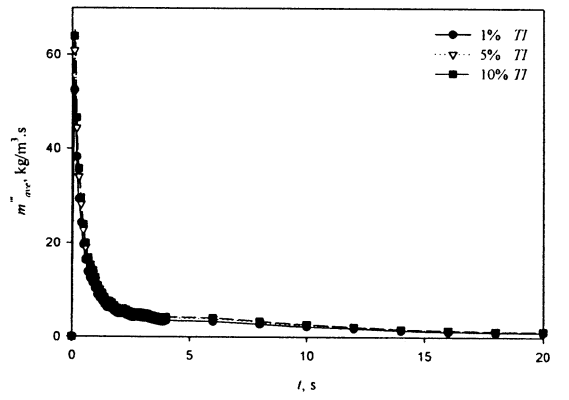

b. Desiccant overall average water adsorption rate

Figure 14. Time dependence of overall average (*a*) water content and (*b*) water adsorption rate in desiccant bed for different turbulent flow intensities: $u_\infty = 1$ m/s, $\mathrm{Re} = 6{,}000$, $T_\infty = 30°\mathrm{C}$, $C_\infty = 0.0276$ kg/kg, $C_b = 0.0075$ kg/kg; $W_o = 0.1$ kg/kg, $L = 0.05$ m, $h = 0.05$ m, $b = 0.00321$ m, $\sigma = 0.1$.

Table 1. Sensitivity of parameters of interest to design variables

Parameters	Change in T	% Change in C	% Change in W_{ave}	% Change in m'''_{ave}
Bed thickness (b) (7–3 mm)	0.11°C/mm	1.3%/mm	0.82%/mm	7.4%/mm
Reynolds no. (Re) (333–3,333)	−0.76°C	36%	50%	88%
Channel width (h) (50–10 mm)	0.9°C	10%	5%	20%
Turbulent intensity (TI) (1–10%)			7%	20%

where ζ represents T, C, W_{ave}, or m'''_{ave}. θ represents b (bed thickness), Re (Reynolds number), h (channel width), or TI (turbulent intensity). The subscripts L and S refer to the largest and smallest values of θ, respectively. When ζ represents T, the change in the temperature (T) is defined as the difference between the largest and the smallest value of ζ for different parameters (θ). For the bed thickness case, the changes in the parameters (ζ) are divided by the value of the difference between the largest and the smallest thickness.

6. CONCLUSIONS

A conjugate model of flow and heat and mass transport for laminar and turbulent humid air flow over desiccant plates and in channels was successfully formulated, solved, and validated.

The results of the fluid dynamics analysis for an external laminar flow are as follows,

- The overshoot in the velocity profile for low Reynolds numbers shown by the numerical analysis was decreased to near zero when the upstream computational domain was increased to $2L$, and was found to decrease as the Reynolds number (Re_L) increased, even without having to extend the computational domain along x.
- Deceleration in the boundary layer progresses along the plate, even generating flow reversal for thicker plates.
- The front and rear edges of the plate in the extended computational domain exhibit stronger mixing and higher heat and mass transfer.

Quantitative magnitudes of heat and mass transport and absorption rates enhancement were given, with use of

- Thinner desiccant beds
- Larger Re, especially when turbulent flow is reached
- Narrower channels or ducts.

REFERENCES

1. H. S. Al-Sharqawi, A Conjugate Transient Computational Analysis of Flow, Heat, and Mass Transfer in Desiccant-Airflow System, Ph.D. dissertation, University of Pennsylvania, May 2002, pp. 226–227.

2. Y. Fujii and N. Lior, Conjugate Heat and Mass Transfer in a Desiccant-Airflow System: A Numerical Solution Method, *Numer. Heat Transfer A*, vol. 29, pp. 689–706, 1996.
3. A. A. Pesaran and A. F. Mills, Moisture Transport in Silica Gel Packed Beds—I. Theoretical Study, *Int. J. Heat Mass Transfer*, vol. 30, pp. 1037–1049, 1987.
4. A. A. Pesaran and A. F. Mills, Moisture Transport in Silica Gel Packed Beds—II. Experimental Study, *Int. J. Heat Mass Transfer*, vol. 30, pp. 1051–1060, 1987.
5. K. D. Kafui, Transient Heat and Moisture Transfer in Thin Silica Gel Beds, *J. Heat Transfer*, vol. 116, pp. 946–953, 1994.
6. J. L. Niu and L. Z. Zhang, Effects of Wall Thickness on the Heat and Moisture Transfers in Desiccant Wheels for Air Dehumidification and Enthalpy Recovery, *Int. Commun. Heat Mass Transfer*, vol. 29, no. 2, pp. 255–268, 2002.
7. W. R. Foss, C. A. Bronkhorst, and K. A. Bennett, Simultaneous Heat and Mass Transport in Paper Sheets during Moisture Sorption from Humid Air, *Int. J. Heat Mass Transfer*, vol. 46, pp. 2875–2886, 2003.
8. Li Yong and K. Sumathy, Comparison between Heat Transfer and Heat Mass Transfer Models for Transportation Process in an Adsorbent Bed, *Int. J. Heat Mass Transfer*, vol. 47, pp. 1587–1598, 2004.
9. F. M. White, *Viscous Fluid Flow*, 2d ed., McGraw-Hill, New York, 1991.
10. V. C. Mei and Z. Lavan, Performance of Cross-Cooled Desiccant Dehumidifiers, *ASME J. Solar Energy Eng.*, vol. 105, pp. 300–304, 1983.
11. C. Chen and S. Jaw, *Fundamentals of Turbulence Modeling*, Taylor & Francis, New York, 1997.
12. S. V. Patankar, *Numerical Heat and Fluid Flow*, Taylor & Francis, New York, 1980.
13. M. Nishioka and T. Miyagi, Measurement of Distribution in the Laminar Wake of a Flat Plate, *J. Fluid Mech.*, vol. 84, pp. 705–715, 1978.
14. J. Caille and J. Schetz, Finite-Element Navier-Stokes Analysis of the Flow about a Finite Plate, *AIAA J.*, vol. 27, pp. 1089–1096, 1989.